University of Colorado / National Centers for Environmental Information IGRF-13 Candidate Models

Patrick Alken[1], Arnaud Chulliat[1], and Manoj Nair[1]

[1]Cooperative Institute for Research in Enviromental Sciences, University of Colorado, Boulder, CO, USA

October 1, 2019

1 Model Parameterization

We define our IGRF-13 candidate models with the usual Schmidt-normalized spherical harmonics and Gauss coefficient parameterization,

$$V(\mathbf{r},t) = R\sum_{n=1}^{N}\sum_{m=0}^{n}\left(\frac{R}{r}\right)^{n+1}\left(g_n^m(t)\cos m\phi + h_n^m(t)\sin m\phi\right)P_n^m(\cos\theta) \quad (1)$$

Here, $R = 6371.2km$, $N = 15$, and the Gauss coefficients $g_n^m(t), h_n^m(t)$ are defined in terms of order 3 B-splines:

$$g_n^m(t) = \sum_{j=1}^{3} g_{n,j}^m N_j(t) \quad (2)$$

$$h_n^m(t) = \sum_{j=1}^{3} h_{n,j}^m N_j(t) \quad (3)$$

The Gauss coefficients, and thus the B-spline basis functions $N_j(t)$ are defined on a 3-year time period close to the desired epoch. For the IGRF 2020 main field and secular variation models, this time period is 2016.71 to 2019.71. For the DGRF 2015 main field, the time period is centered on 2015: 2013.5 to 2016.5. The B-spline functions $N_j(t)$ are order 3 and defined with no interior knots. This means the Gauss coefficients $g_n^m(t), h_n^m(t)$ are quadratic polynomials spanning the 3 year time window. Since there are 3 control points for each spline, there is a one-to-one correspondance between each spline and a Taylor series expansion over the 3-year time interval.

2 Data Description and Preprocessing

We use data from the Swarm A and B satellites to build all 3 candidate models. The Swarm data was preprocessed to select data with at least two operating star cameras, geomagnetically quiet data (with Kp less than 2 and $|dRC/dt| < 3nT/hour$. Also mid-latitude (equatorward of 55 degrees QD latitude) tracks were only used when the ascending node local time was between midnight and 500AM. At high-latitudes (poleward of 55 degrees QD latitude), data was only used when the sun was at least 10 degrees below the horizon. Swarm vector measurements were used between $\pm 55^\circ$ QD latitude, while scalar data were used at all latitudes.

Since IGRF requires only a main field to SH degree 13, we removed the MF7 crustal field model (degrees 16-133) from the Swarm data as a preprocessing step. We additionally removed the CHAOS-6 external (magnetospheric) field model, based on the RC index from the Swarm measurements. As mentioned previously, the time period used for the three models is given in the table below.

Model	Start Time	End Time
DGRF MF 2015	2013.50	2016.50
IGRF MF 2020	2016.71	2019.71
IGRF SV 2020	2016.71	2019.71

3 Model Building and Fit Statistics

The models were built by minimizing the residuals between the data and internal potential field model described above. A nonlinear Levenberg-Marquardt algorithm was used with robust iterative reweighting to minimize the effects of outliers on the final model. After determining the Gauss coefficients to SH degree 15, the main field models were made by truncating the parent model to SH degree 13, while the SV model was made by truncating the parent model to SH degree 8. We regularized the models by minimizing the 1st and 2nd time derivatives of the B_r component, averaged over the core mantle boundary. The regularization parameters were chosen to achieve a nice visual convergence of the SH coefficients in the Lowes-Mauersberger spectral plots (see Sec. 4). We built two models, labelled A and B, where model A had slightly larger SV (1st derivative) damping, while model B had less. After a validation study, we opted to choose model B as our final candidate (see Sec. 4).

The fit statistics of the parent model for each satellite are given in Tables 1 and 2.

4 Validation

4.1 Model Comparisons

We validated our IGRF candidate models by doing spectral and spatial comparisons with other models, such as CHAOS-6, as well as comparisons with

Component	N	mean (nT)	sigma (nT)
X	67436	-0.90	4.34
Y	67436	0.02	2.82
Z	67436	0.00	2.03
low/mid-latitude F	67447	-0.44	2.85
high-latitude F	29478	0.81	8.02

Table 1: Swarm A statistics

Component	N	mean (nT)	sigma (nT)
X	76162	0.48	5.29
Y	76162	0.09	2.95
Z	76162	0.04	2.46
low/mid-latitude F	76180	0.15	3.34
high-latitude F	29835	0.94	7.03

Table 2: Swarm B statistics

observatory datasets. We compared two different IGRF2020 NCEI candidate models, labelled A and B. The difference between the two is only a small difference in SV regularization. Figure 1 shows the Lowes-Mauersberger spectra comparing candidate models A and B with CHAOS-6-x9. Model B, which was given less SV regularization, is closer to the CHAOS-6-x9 SV spectrum. This is the main reason we selected Model B as our final candidate model for the 2020 epoch.

Figure 2 shows a spatial map of the differences in the B_r component between Model B and CHAOS-6-x9 at the 2020 epoch. We find differences of up to 20 nT in certain parts of the world, especially the antarctic region. These differences are likely due to differences in regularization (CHAOS-6 regularizes the endpoints of the Gauss splines, while our approach does not). Additionally, CHAOS-6-x9 used Swarm data only through April 2019. Figure 3 shows a spatial maps of the differences in SV between Model B and CHAOS-6-x9 at the 2020 epoch. We find differences of up to 25 nT/year in certain regions, which we again attribute to regularization differences and data availability for the two models. Overall, we believe our model is reasonably consistent with the predictions of CHAOS-6-x9, extrapolated to 2020.

4.2 Observatory Comparisons

Our aim here is to compare the candidate secular variation models with a global set of geomagnetic observatory data. We use hourly mean database of geomagnetic observatory data compiled by the British Geological Survey for years 2006-2019 (update of September 2019). We limit the observatories to those located below geomagnetic latitudes of ± 55. Observatories with baseline errors, large data gaps were omitted from the analysis. A total of 42 geomagnetic observatories, distributed across the world, were available for the analysis (Figure 4).

Model	SV Epoch	X rms (nT/yr)	Y rms (nT/yr)	Z rms (nT/yr)
IGRF13 A	2020	20.71	10.14	14.08
IGRF13 B	2020	20.72	10.54	14.07

Table 3: root-mean-square differences between observed and predicted SV at observatories

Most of the observatories have data coverage up to June 15, 2019 (range March 24, 2019 to August 29, 2019). We select data for geomagnetically quiet condition ($ap \leq 10$) and limit the analysis to 0-5 LT to reduce the influence of disturbance signals. We fit cubic splines with knots separated by 1 year separately to X, Y and Z components in a least-square sense. Secular variation at an observatory was determined by subtracting the spline value at the beginning and end of a year centered on the SV year of the model. We then find the global mean and root-mean-square (RMS) of the differences between model and prediction. The RMS errors were calculated after the global means were removed from all the differences (Table 3).

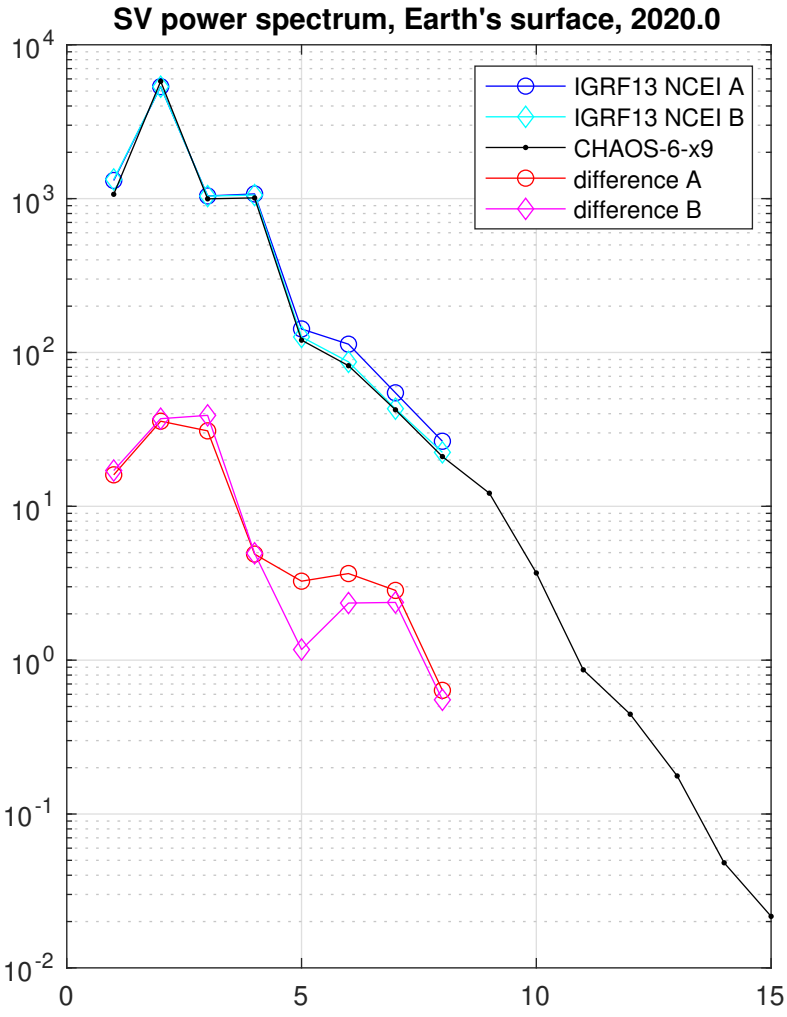

Figure 1: Spectral comparisons of SV 2020 candidate models with CHAOS-6-x9

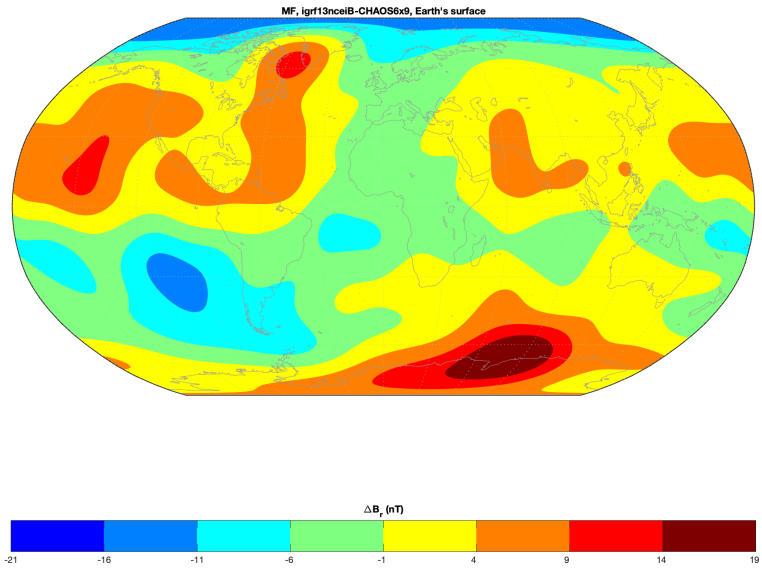

Figure 2: Surface map of differences in B_r between Model B and CHAOS-6-x9, 2020 epoch

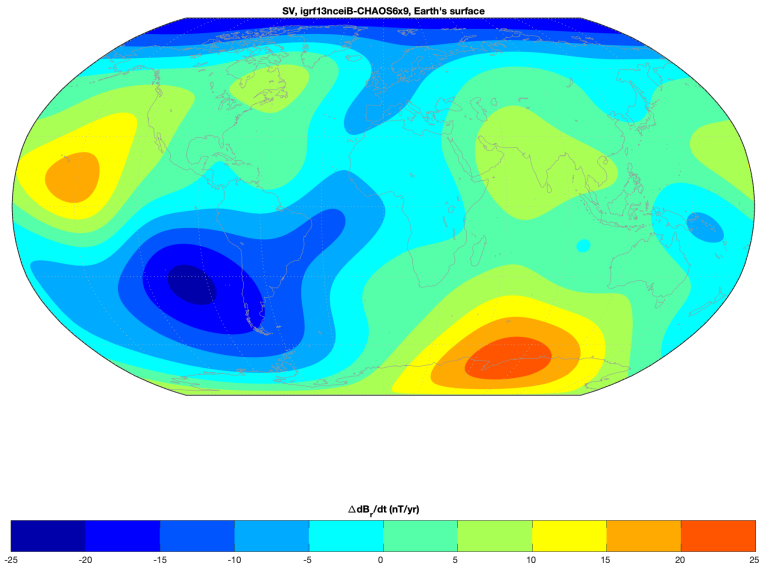

Figure 3: Surface map of differences in dB_r/dt between Model B and CHAOS-6-x9, 2020 epoch

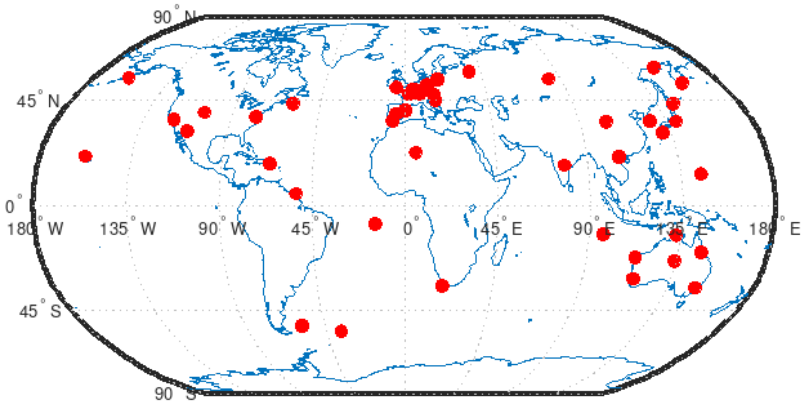

Figure 4: Observatories used for SV analysis